Taylor & Francis
Taylor & Francis Group

MICROCHANNEL HEAT SINKS: AN OVERVIEW OF THE STATE-OF-THE-ART

I. Hassan, P. Phutthavong, and M. Abdelgawad

Department of Mechanical and Industrial Engineering, Concordia University, Montreal, Quebec, Canada

Computers are rapidly becoming faster and more versatile, and as a result, high-powered integrated circuits have been produced in order to meet this need. However, these high-speed circuits are expected to generate heat fluxes that exceed the circuit's allowable operating temperature, and so an innovative cooling device is needed to solve this problem. Microchannel heat sinks were introduced in the early 1980s to be used as a means of cooling integrated circuits. Since then, many studies have been conducted in the field of these microchannel heat sinks. Earlier research used mainly single-phase coolants in their heat sinks, but two-phase coolants are now the focus of more recent research. The purpose of this article is to present a state-of-the art literature review of the progress of research in the field of microchannel heat sinks. This literature will focus mainly on the most recent research, starting with the latter half of the 1990s.

INTRODUCTION

Today's electronic components are required to perform tasks at a faster rate, and so high-powered integrated circuits have been produced in order to meet this need. These high-speed circuits are expected to generate heat fluxes that will cause the circuit to exceed its allowable temperature. In order to solve this problem, microchannel heat sinks were introduced in 1981 by Tuckerman and Pease [1] and have since been the study of many researchers in the field of fluid mechanics. Microchannel heat sinks function in a rather simple manner. Multiple microchannels are machined on the back of the substrates of electronic components in integrated circuits. The heat generated by the electronic component is transferred to the coolant by forced convection. The microscopic size of the channels causes a decrease in the thickness of the thermal boundary layer, which generates a decrease in the convective resistance to heat transfer, thus generating high cooling rates.

In the 1980s, Tuckerman [2] suggested that laminar flow is the best for heat removal through microchannels, due to the development of the thin thermal boundary layer. He designed microchannel heat sinks with different dimensions in order to study flow friction

NOMENCLATURE

b	slip coefficient	Z	effect of aspect ratio $=$ min $(H, L)/\max(H, L)$
D	microchannel diameter (m)		
f	friction factor		
h	heat transfer coefficient (W/m$^2 \cdot$ °C)	**Greek Symbols**	
$\overline{h}$	average heat transfer coefficient (W/m$^2 \cdot$ °C)	λ	mean free path of molecules (m)
		μ	dynamic viscosity (Pa $\cdot$ s)
H	microchannel height (m)	ρ	density (kg/m^3)
k	thermal conductivity (W/m $\cdot$ °C)	σ	surface tension (N/m)
Kn	Knudsen number	σ_v	tangential momentum accommodation coefficient
ℓ	characteristic length (m)		
L	microchannel length (m)		
Nu	Nusselt number $\left(= \frac{\overline{h}L}{k}\right)$	**Subscripts**	
Pr	Prandtl number	c	channel
q_w	wall heat flux (W/m^2)	CHF	critical heat flux
Re	Reynolds number $\left(= \frac{\rho U \ell}{\mu}\right)$	e	thermodynamic equilibrium
		l	along length
T	temperature (°C)	tp	two-phase
U	velocity (m/s)	v	vapor
w_c	microchannel width (m)	w	wall
x	quality		

and heat transfer within these sinks. He also developed an optimization procedure to predict the best aspect ratio of the channel to achieve the best heat transfer. He used only liquid water as a coolant in his experiments. When examining the flow friction, he discovered that head loss was much larger than he anticipated. Also, the value he obtained for the thermal resistance, defined as $\Delta T/q_w$ for one-dimensional heat flow, was more than 20 times lower than other cooling devices used for cooling integrated circuits at the time. Since Tuckerman's work in the 1980s, many investigations have been conducted with the purpose of gaining further understanding of the fluid mechanics within microchannel heat sinks. The study of heat transfer and fluid flow in microchannel heat sinks can be divided into two subsections, depending on the phase of the coolant that flows through them. These are single-phase flow and two-phase flow. The present literature review will provide the progress of the study of heat transfer and fluid flow in each section and will ultimately lead to new future research directions in the field. It will focus mainly on the recent benchmark research, starting with the latter half of the 1990s.

SINGLE PHASE FLOW

Liquid Phase

Earlier research focused mainly on single-phase liquid flow. In 1998, Poh and Ng [3] conducted a numerical analysis of fluid phenomena in microchannel heat sinks using ANSYS, a CFD package, by simulating flow in a microchannel array. They used Fluorocarbon Liquid FX-3250, which boils at 56°C. Sixteen different situations were studied whereby the microchannel width, height, length, the inlet velocity of the coolant, and the wall heat flux were varied. For simplicity, only half the microchannel width was considered for their numerical study. The values for half the microchannel width

were $0.5w_c = 28.3$ and 56.6 μm and the microchannel heights used were $H = 150$ and 200 μm. The lengths of the microchannels were $L = 400$ and 1000 μm and the coolant velocities utilized were $U = 0.1$ and 1.0 m/s. The wall heat fluxes imposed on the microchannel heat sink were $q_w = 2.48 \times 10^5$, 3.17×10^5, 4.42×10^5, and 5.49×10^5 W/m^2. They assumed laminar flow, constant fluid properties and inlet velocity, uniform wall heat flux, as well as zero pressure and zero velocity gradients at the exit of the microchannel. The wall opposite to the isoflux wall was considered adiabatic. Poh and Ng showed that the effect of the microchannel length was slight, where a decrease in length caused an increase in thermal resistance. Similarly, the thermal resistance increased when decreasing the microchannel depth, increasing the width, and decreasing the inlet velocity. Their numerical results were compared with available analytical results and proved to be in good agreement.

In 1998, Kawano et al. [4] performed both experimental and numerical studies of pressure drop and heat transfer in microchannel heat sinks. For their experiments, 110 microchannels were arranged in a microchannel heat sink of a 15×15 mm^2 area. Water served as the coolant. The microchannel width was fixed at 57 μm, and the height used was either 180 or 370 μm, depending on the phenomena under investigation. Fully developed laminar flow was assumed in the numerical simulations. The microchannel heat sink was not heated for the pressure drop measurements. The pressure drop results of the experiments and simulations were in good agreement with each other for $0 < \text{Re} < 200$. In this range, the values for the thermal resistances at the entrance of the microchannel varied by quite a large margin. This discrepancy was attributed to the fact that viscosity of the water is dependent on temperature, and that there is a large temperature gradient at the inlet. For $\text{Re} > 300$ the predicted values of the pressure drop in the simulation were lower than those obtained in the experiments. The thermal resistance change across the heat sink (from entrance to exit) was approximately 0.1 K/W $\cdot$ cm^2, which indicates that the temperature difference was about 10 K for a heat flux of 100 W/cm^2. Hence, larger heat fluxes may generate enough thermal stress to break the chip if careful design is not performed.

Zeighami et al. [5] studied transition from laminar to turbulent flows for water in microchannel heat sinks. Previous work indicates that flow transition occurred at a transition Reynolds number lower than 2200, which is the transition Re at the macroscale. Low transition Reynolds numbers could be due to surface roughness, viscous heating, and/or the electric double layer. Until now, analytical work has not been able to determine the transition Reynolds number at the microscopic level. This transition number can only be studied experimentally. Using microresolution particle image velocimetry, Zeighami et al. generated vector fields in a microchannel measuring 150 μm $\times$ 100 μm $\times$ 1 cm. Velocity fields at Reynolds numbers of 200, 720, 1200, and 1600 were generated. Except for the case where $\text{Re} = 1600$, all fields seemed steady and parallel. When $\text{Re} = 1600$, the flow began to show some turbulent behavior. The velocity fields temporally fluctuated and became more asymmetric.

Rahman [6] experimentally determined the pressure drop and heat transfer in two different geometries of microchannel heat sinks. The two configurations are I-channels, where the working fluid flows through parallel channels, and U-channels, where the fluid passes through numerous bends in a single channel. The width of the individual channels was 1 mm and the depths ranged from 176 to 278 μm. Using water as the coolant, he measured the pressure and temperature of the coolant along the microchannel. Rahman's
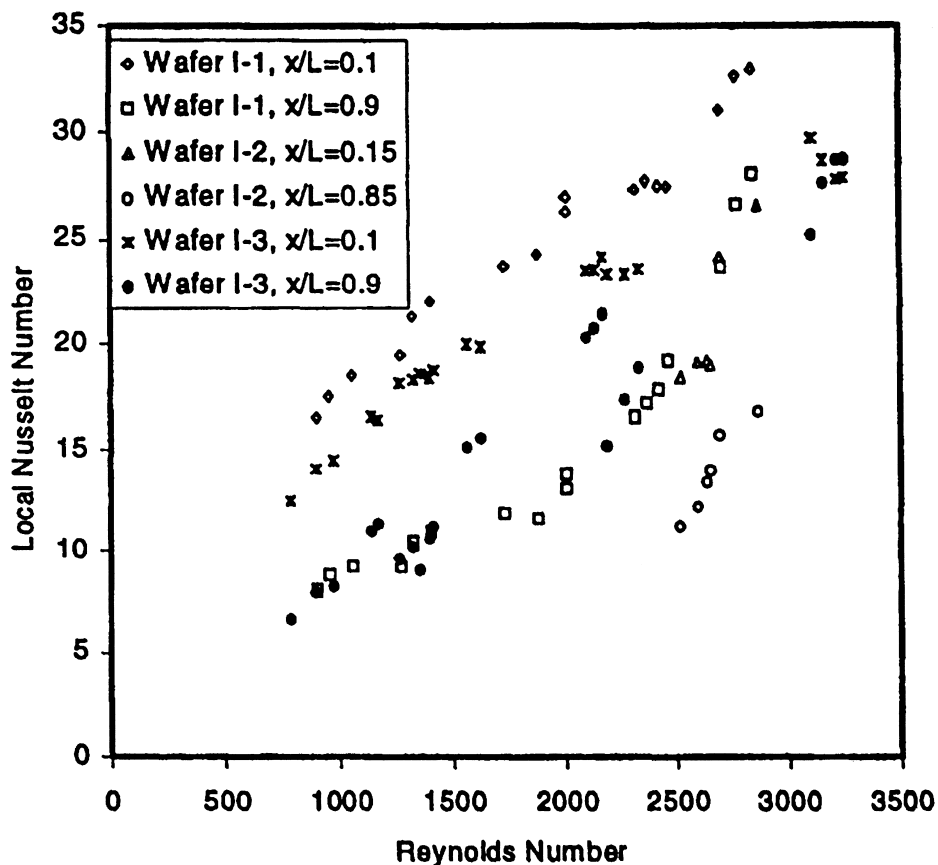
Figure 1. Variation of the local Nusselt number with Reynolds number at various locations in I-channels [6].

results showed that the Nusselt number is always greatest at the entrance for any value of Reynolds number as shown in Figure 1 (I-channels). This was expected since the boundary layer is beginning to form at the entrance. In addition, it seemed that the flow transitions from laminar to turbulent is very gradual because of the microscopic dimensions. He concluded that the average Nusselt number in microchannels is higher than in larger channels because the velocity boundary layer breaks down due to the surface roughness of the microchannel walls.

Li et al. [7] studied the effect of surface roughness on the transition Reynolds number in microchannels. They conducted experiments using stainless steel microchannels with diameters of 128.8, 136.5, and 179.8 μm and relative surface roughness between 0.03 and 0.043. Their results showed that for theoretical values of Reynolds numbers ranging from 500 to 2000, the friction factor was approximately 10 to 25% higher in value. The transition Reynolds number from laminar to turbulent flow was approximately 1800.

In 2003, Guo and Li [8] presented their comprehensive study of the effect of microdimensions on the surface friction factor in microchannels. In their experiments,
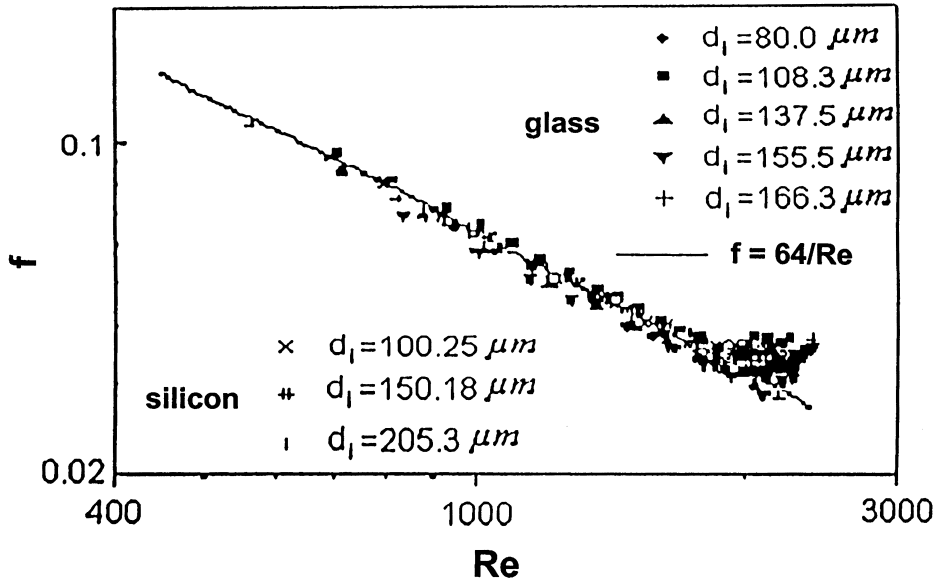
Figure 2. Friction factor in smooth microchannels with water as the working fluid [8].

smooth glass and silicon microchannels were used with diameters ranging from 80 to 166 μm, with water as the working fluid. Their results are shown in Figure 2, where for smooth microchannels the product of the friction factor and Reynolds number is approximately equal to 64, which is the case for flows in conventional sized tubes. Also, the Reynolds number at which the transition from laminar to turbulent flow occurs is between 2000 and 2300. However, flow through rough microchannels does not behave in the same manner.

Gao et al. [9] also studied the transition Reynolds number in microchannels by investigating how it varies with the channel height. The channel width and length was fixed at 25 mm and 82 mm, respectively, while the channel height ranged from 0.1 mm to 1 mm. The accepted transition Reynolds number for plane wall channels is 4000, and from the results presented in Table 1, the transition Reynolds number is virtually not affected by the channel height. The largest difference occurs for larger channel heights,

Table 1. Critical Reynolds number at various microchannel heights

Microchannel Height, e (mm)	Critical Reynolds number
1	2200
0.7	3300
0.5	3400
0.4	3400
0.3	3500
0.2	2300

From Gau et al. [9].

which Gao et al. concluded was the result of experimental uncertainties due to the increase in pressure drop as a result of increasing the channel height.

Riehl et al. [10] presented the available correlations that may be used to predict the heat transfer coefficients in single-phase and two-phase flows. Peng and Wang [11, 12] developed two correlations for the Nusselt number in single-phase and boiling flows for water. These correlations are, respectively, as follows:

$$\mathrm{Nu} = 0.00805 \mathrm{Re}_l^{0.8} \mathrm{Pr}_l^{1/3} \tag{1}$$

and

$$\mathrm{Nu} = 1.86 \mathrm{Re}_l^{1/3} \mathrm{Pr}_l^{1/3} \left(\frac{D}{L}\right)^{1/3} \left(\frac{\mu_l}{\mu_v}\right)^{0.14} \tag{2}$$

They observed no partial nucleate boiling in microchannel flows. Peng and Peterson [13, 14] also used water as a coolant and developed the following correlation experimentally:

$$\mathrm{Nu} = 0.072 \left(\frac{D_h}{W_c}\right)^{1.15} [1 - 2.42(Z - 0.5)^2] \mathrm{Re}_l^{0.8} \mathrm{Pr}_l^{1/3} \tag{3}$$

When the correlation was used to predict data from another investigation, the maximum deviation was 25%.

In 1999, Ng et al. [15] generated a numerical model for flow and heat transfer in one microchannel of a microchannel heat sink, using the STAR-CD CFD software. They assumed uniform pumping and a uniform heat flux of 500 W/cm^2. They also assumed that the flow was incompressible and laminar. The temperature of the water at the inlet of the microchannel was set to 20°C, and its velocity was fixed at 1.0 m/s. The microchannel dimensions were: $w_c = 250$ μm, $H = 1000$ μm, and $L = 1.0$ cm. They showed that the wall temperature of the microchannel increases in the direction of fluid flow, ultimately attaining a maximum temperature of 172.9°C at the outlet of the microchannel. The total pressure drop was 2.66 kPa and the maximum thermal resistance was 0.3 K/W · cm^2.

In 1999, Fedorov and Viskanta [16] generated a three-dimensional theoretical model for heat transfer in an asymmetric rectangular microchannel. The x-direction is the flow direction, the y-direction is the width direction, and the z-direction is the height direction. The purpose was to determine the effect of coolant type, solid substrate material, and channel geometry on the heat transfer in a microchannel heat sink. The flow was assumed to be steady state, three-dimensional, laminar, and incompressible. The thermophysical properties of the coolant were assumed to be dependent on temperature. For boundary conditions, all outside walls except the right Z-wall were considered adiabatic with no-slip boundary conditions. A constant heat flux, $q_w = 90$ W/cm^2, was applied to the right Z-wall. Uniform velocity and temperature at the inlet were defined, and the gradients of both were set to disappear at the outlet of the microchannel. The results from their model showed good agreement with available experimental data, hence they concluded that it could be used to predict the behavior of flow and heat transfer in microchannel heat sinks. Water, fluorocarbon dielectric fluid FC-77, and air were used in their simulations, and water was shown to be the best. For the channel geometry, larger aspect ratio channels were found to operate at much lower temperatures for the same heat dissipation.

Fedorov and Viskanta continued their work a year later [17]. Using the same assumptions and physical model as they did in the study mentioned above, they studied subsequent three-dimensional heat transfer in an asymmetric rectangular channel when the right Z-wall is heated. Their analyses concluded that the heat introduced at the right Z-wall is transferred to the remaining channel walls through conduction, moving in the upstream direction toward the inlet of the microchannel. Heat transfer to the coolant is at its maximum at the inlet since there is minimum convective resistance. Due to the smaller spacing between the two Y-walls, the heat flux at these walls is two orders of magnitude higher than that at the Z-walls. At the corners of the microchannels the boundary layers interact and produce competition between two local thermal resistances: one for the heat transfer of one wall to the bulk fluid, and the other for the heat transfer between the two adjacent walls via the corner boundary layers. The heat will be conducted through adjacent walls, rather than being convected to the bulk fluid because the conduction thermal resistance is smaller than that produced by heat transfer through convection. As a result, the heat from the Z-wall passes through the fluid and meets the adjacent Y-wall, producing heat vortices at the corners of the microchannel. Thus, the heat transfer coefficient is an inadequate parameter to define heat transfer in conjugate problems.

Perret et al. [18] developed an optimization model that could be used to determine the best parameters suited for microchannel heat sinks. Water was chosen as the coolant because of its high specific heat capacity, which in turn minimizes capacitive resistance. They generated analytical models to determine relationships between the thermal resistance of the heat sink and the heat sink's dimensions. The dimensions of the microchannel heat sinks were varied such that the value of the heat transfer coefficient, in the analytical models they produced, was optimized. This was accomplished by using a home-developed software entitled Pascosma. Perret et al. indicated that fabrication of the optimized microchannel heat sink is still ongoing. Thus, experimental work needs to be conducted on the optimized heat sink to determine whether it really yields the best performance.

Gas Phase

In conventional sized channels, gas flow is assumed to be incompressible as long as the Mach number is much smaller than unity. However, at the microscale level, as reported by Guo and Wu [19, 20] there is significant variation in the density of gases due to the large pressure drops resulting from the surface friction inside the microchannels. Most studies of heat transfer and fluid flow in microchannel heat sinks use liquid coolants, as opposed to gaseous coolants. However, there are some studies that utilized gaseous coolants, such as air, and a summary of recent investigations is presented below.

In the same experiment described in the Liquid Phase section, Guo et al. [8] studied gas flow in the same microchannels with diameters ranging from 80 to 166 μm. As shown in Figure 3, for Mach numbers less than 0.3, the friction factor behaves in the same manner as conventional sized channels where $f \cdot \text{Re} = 64$. For Mach numbers above 0.3, the friction factor increases due to the flow compressibility caused by the surface friction.

In 1996, Marongiu [21] presented the parameters that limit the design of gas-phase microchannel heat sinks. The use of gas coolants is limited by the onset of frictional and thermal choking, as well as the formation of shocks. Supersonic micropockets with
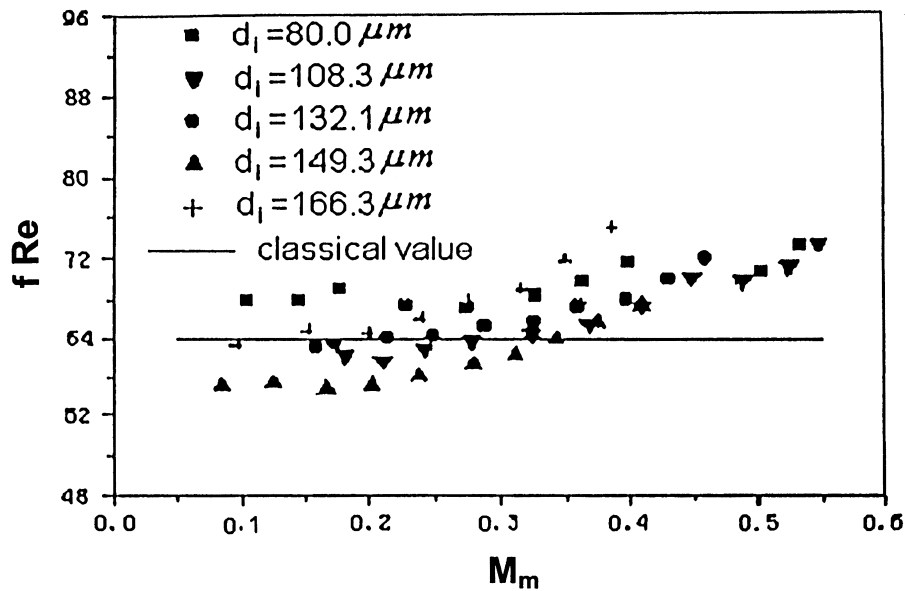
Figure 3. Variation of friction factor with Mach number for gas flow in smooth microchannels [8].

shock waves need to be evaded to avoid increasing pumping power and damaging the channel. Also, Mach number will inevitably increase because of friction and heat addition; therefore compressibility effects must be considered. Now, sonic flow will occur at a certain length of the microchannel. As the length of the channel is increased, the flow rate will decrease, reducing the cooling performance of the sink. In addition, excessive pressure drops must be avoided to circumvent choking. Moreover, there is a maximum quantity of heat that a gas-cooled microchannel heat sink may dissipate because heat addition could render the flow sonic at the outlet. Finally, it is important not to include too many microchannels for gas coolants, because the heat transfer decreases for a given volumetric flow rate as the number of channels increases.

In 1998, Marongiu et al. [22] designed a board composed of channels through which air flows at speeds greater than 50 m/s. The board had a length of 0.15 m, a height of 0.025 m, and a width of 0.1 m. All the channels were 2 mm thick. The efficiency of the heat sink was determined by measuring the degree of irreversibilities by obtaining the local stagnation pressure. Results showed that heat removal rates are greater at higher speeds. However, choking occurred at some point in the apparatus at air speeds of approximately 50 m/s.

It is important to consider the flow regime, velocity slip, and temperature jump boundary conditions when dealing with gaseous flow in microchannels. The Knudsen number, $Kn = \frac{\lambda}{\ell}$, determines the flow regime; these flow regimes are the continuum flow regime, slip flow regime, transition flow regime, and free-molecular flow regime. The flow equations and boundary conditions that may be applied for a certain flow depends on its flow regime. Beskok and Karniadakis [23, 24] developed a unified model to predict the mass flow rate and pressure distribution in channels, pipes, and ducts for Knudsen numbers, Kn, ranging from zero to infinity. A new second-order general velocity slip

boundary condition was introduced in order to develop this model. They compared their new model with existing results obtained though DSMC (Direct Simulation Monte Carlo) simulations, linear Boltzmann solutions, and experimental data.

The general velocity slip boundary condition predicts the amount of velocity slip in channels for all flow regimes as follows:

$$U - U_w = \frac{2 - \sigma_v}{\sigma_v} \left[\frac{Kn}{1 - bKn} \left(\frac{\partial U}{\partial n} \right) \right] \tag{4}$$

where U is the gas velocity, U_w is the wall velocity, σ_v is the tangential momentum accommodation coefficient, and $\partial U/\partial n$ is the derivative tangential velocity in the direction normal to the solid surface. The slip coefficient, b, may be obtained through experimental data, linear Boltzmann data, or DSMC data. Now, the unified flow model enables the prediction of the velocity profiles, pressure drops, and mass flow rates for flows in channels, pipes, and all arbitrary aspect ratio rectangular ducts, for flows in all flow regimes; that is, $0 \leq Kn \leq \infty$. First, the shape of the velocity profile is predicted using velocity scaling. Velocity scaling showed that assuming the velocity profile in a channel is parabolic is a good approximation in the continuum, slip, and free-molecular regime. Figure 4 shows
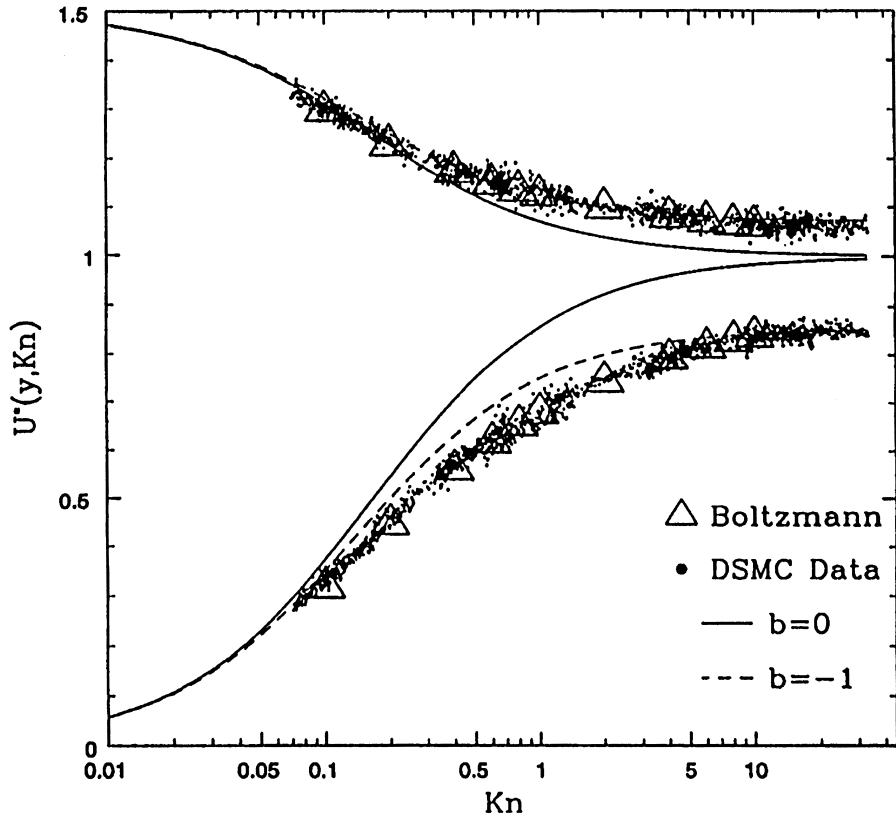

Figure 4. Comparison of velocity distributions normalized with the average velocity along the centerline and wall of the microchannel [23].

the nondimensionalized velocity distribution at the wall and along the centerline of the microchannel for $0.01 \leq \text{Kn} \leq 30$. It can be seen that Maxwell's first-order boundary condition ($b = 0$) is erroneous for large Knudsen numbers, where it predicts a uniform velocity distribution. The slip flow theory breaks down for $\text{Kn} = 0.1$ for the wall velocity and for $\text{Kn} = 0.4$ for the centerline velocity, and so accounts for this error. For the second-order boundary condition ($b = -1$), the model slightly overpredicts the DSMC data for $0.1 \leq \text{Kn} \leq 5$, and this is mostly likely due to the effect of the Knudsen layer. Thus, in the transition flow regime there are some slight deviations due to the development of the Knudsen layer. Next, the actual magnitude of the average velocity, and thus the volume flow rate, are obtained through flow rate scaling. The model was validated by comparing their results with existing DSMC data in the slip/early transition regimes. As rarefaction increases, the curvature in the pressure distribution decreases until it becomes almost linear.

In 1996, Baker and Calvert [25] conducted a numerical study on the temperature-dependent nature of viscosity on microchannel flows to study the effect of fluid property variation on heat sink performance. Poiseuille flow and linear pressure gradients were assumed, and velocity and temperature were considered to vary only in the lateral direction. Sutherland's model for dynamic viscosity was used, along with the coupled momentum and energy equations. Maxwell's velocity slip boundary condition and Smoluchowski's temperature jump boundary conditions were applied at the solid-fluid interface. Higher-order terms were neglected for the numerical and analytical models. When incorporating variable viscosity, the numerical results in Baker and Calvert's work showed significant differences from the analytical results. More particularly, the variable viscosity model generally yielded results for the temperature distribution, skin friction coefficients, and Stanton numbers that were lower in value compared to the analytical models, although the difference was quite small for the skin friction coefficients. When the Knudsen numbers increased, the velocity and temperature profiles showed no qualitative difference, and the skin friction coefficients and Stanton numbers increased accordingly as well. In addition, increasing certain parameters sometimes yielded nonphysical values in the analytical and numerical models. Thus, higher-order terms must be integrated into both the analytical and numerical models in order to avoid this situation.

TWO-PHASE FLOW

Single-phase flow in microchannel heat sinks requires either high flow rates or smaller hydraulic diameters, consequently resulting in larger pressure drops. Therefore, two-phase microchannel heat sinks are an alternative to single-phase microchannel heat sinks because latent heat can be used to maintain the sink at a uniform temperature

In 1999, Jiang et al. [26] investigated the effect of forced convection boiling on the performance of four different microchannel heat sinks, all with different dimensions less than 100 μm. In all cases, the onset of critical heat flux was determined to study the effect of boiling. DI water was used as the coolant. Qualitatively, it appears that for the smaller sink the temperature increases and then slowly decreases. The opposite occurs for the larger microchannel heat sinks where the temperature decreases initially and then increases. They observed the critical heat flux (CHF) while varying the flow rate of the coolant. Their results showed an almost linear relation for the smaller heat sinks with 40 μm hydraulic diameter channels, where the CHF temperature increases with

increasing with flow-rate. However, the CHF temperature did not appear to vary with flow rate or number of channels for the sinks with 80 μm hydraulic diameter channels, even though inlet pressure increases as the flow rate increases. In addition, no boiling plateau was observed in the boiling curves.

In a later study, Jiang et al. [27] used transparent microchannel heat sinks to observe the flow pattern of the coolant in order to better understand the boiling process. DI water was once again used in their investigations. The hydraulic diameters of the triangular microchannels were 26 μm and 53 μm. Three zones were observed in the boiling curve, and there was no boiling plateau as shown in Figure 5. Zone I was associated with low power input to heat sink, $q/q_{CHF} < 0.4$, where the flow was single-phase liquid from the entrance to the exit of the sink. Local nucleation boiling was observed in this zone but produced negligible differences in the boiling curve. Zone II corresponds to moderate input power, $0.4 < q/q_{CHF} < 0.6$, bubbles larger than the channel's dimensions were formed at the device's common entrance. The bubbles entered the channel only when the pressure was high enough, and thus exited at very high speeds. At the critical value of $q/q_{CHF} = 0.6$, there is annular flow and the flow is unstable due to the random appearances of liquid droplets inside the vapor core. For high input power, $0.6 < q/q_{CHF} < 0.9$, the annular flow becomes stable. A thin film of liquid lined the walls of the microchannels as well as the exterior of the vapor core. Heat transfer was most active at the liquid film-vapor core interface. When approaching CHF conditions, $q/q_{CHF} = 1$, the liquid film totally evaporates, implying that the temperature of the sink increased abruptly, rendering it impossible to continue inputting power beyond the CHF conditions.
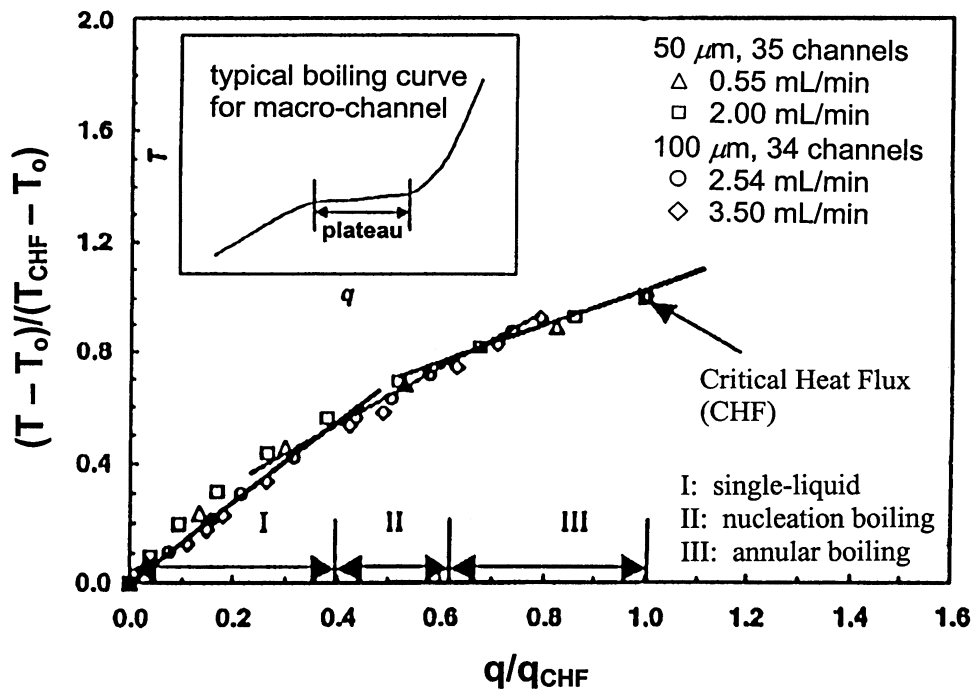

Figure 5. Boiling curve for microchannels [27].

Koo et al. [28] studied, theoretically, two-phase microchannel heat sinks where the hydraulic diameters of the microchannels were less than 100 μm. The wall thickness was fixed at 100 μm, and the channel width and depth were varied between 50 and 250 μm. The flow was divided into four sections. In Section A, the coolant at the inlet is single-phase liquid. Section B is called the flow eruption regime where the coolant undergoes extremely rapid phase change. The flow in this regime is very unstable, such that the vapor onset point oscillates erratically in the longitudinal direction. No transition flow regimes, such as bubbly and plug-flow were observed; thus, Section C is an annular flow regime. Section D exists when the channel is of adequate length and there exist high rates of heat absorption within the microchannel. Complete dryout of the liquid occurs in Section D, and so it is composed entirely of vapor. The erratic behaviors of the flow in Section B, as well as the velocity of the thin film of liquid in Section C, are neglected. Using the finite volume method, Koo et al. solved the energy equations and compared their results to available experimental data. The pressure drop predictions were in good agreement. When the coolant is liquid, the pressure drop decreases as the input power is increased. However, at the onset of two-phase flow, the pressure drop rises quickly as the heating rate rises. As the dimensions of the microchannels increase, the pressure drop decreases. It seems smaller dimensions yield a higher heat transfer coefficient; however, the pressure drop will significantly increase for these smaller dimensions, causing a subsequent increase in the saturation temperature at the onset of two-phase flow.

Zhang et al. [29] studied two-phase forced convective flow in microchannels with hydraulic diameters ranging between 25 and 60 μm. Two devices were fabricated for this study. Device 1 is a multichannel device with 40 channels, and device 2 is a single channel device. DI water is used as the working fluid, and is pumped though the devices at 0.1 ml/min. To account for two-phase flow, a phase change simulation was developed. The simulation considered one-dimensional flow and heat transfer, and its results were compared with the experimental data obtained in this study. The simulation utilized the finite volume method and considers fluid properties that are temperature and pressure dependent. In the single-phase region for device 1, the pressure decreases as the heat power is raised, which is indicative of the lowering of the liquid viscosity due to the increasing temperature. At the onset of boiling, there is acceleration in the local volume flow rate since the density of the vapor is very low compared to that of water. As a result, there is a large pressure drop across the channel. The plot of wall temperature versus heat power shows that the wall temperature decreases slightly at the onset of boiling. Zhang et al. attribute this to nucleation, bubble departure, and possibly pressure fluctuations.

The experimental results for device 2 showed slight differences from those of device 1. Figure 6 shows the pressure curves for device 2 obtained through experimental measurements and through simulations of the annular flow model and homogeneous flow model. When compared to the pressure curves of device 1, it can be seen that the pressure curves for both devices are similar except that boiling begins at lower input heat power, which indicates larger heat loss in device 1. Boiling instability occurs due to the large drop in pressure at regions where the flow undergoes phase transition. The fluid reverts back to liquid and begins to boil once again. The cycle lasts up to a few minutes. Device 2 showed no decrease in wall temperature occurred at boiling. The wall temperature profiles for both devices were parabolic, demonstrating that there is more heat loss through conduction at the inlet and outlet. Small bubble growth occurred in the microchannels with hydraulic diameters less than 60 μm. Annular flow was observed with an extremely thin layer of liquid. Bubbly flow and plug flow were not observed.
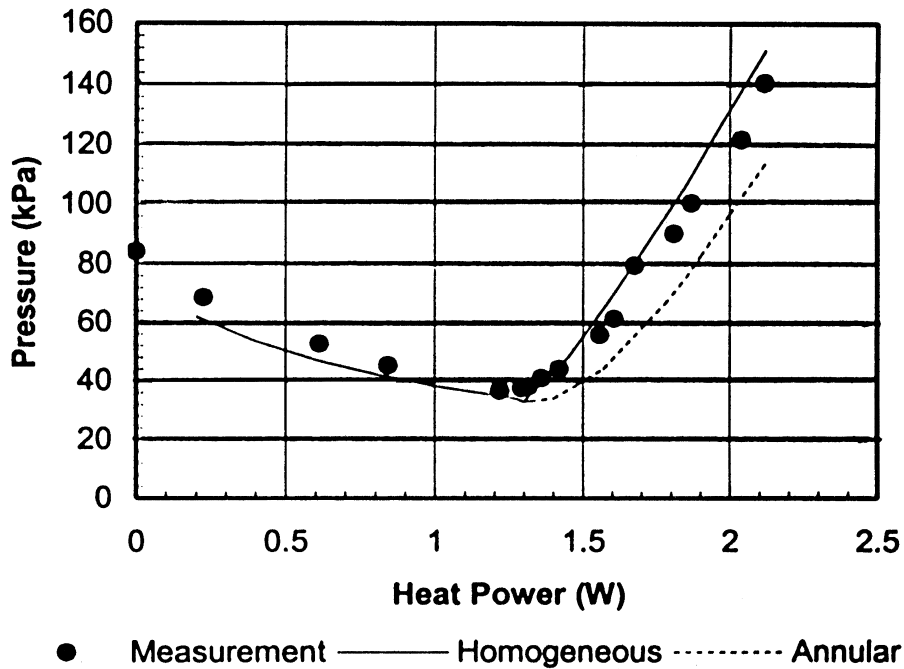
Figure 6. Variation of pressure with heat power for various models for two-phase flow in microchannels [29].

In a later study, Zhang et al. [30] investigated nucleate boiling conditions in microchannels with hydraulic diameters less than 150 μm by performing experiments on channels with different surface textures and using DI water of various surface tensions. Zhang et al. had previously observed that for channels with hydraulic diameters greater than 100 μm, bubbles grow on the channel walls and annular flow eventually develops at higher heat fluxes. For channels with hydraulic diameters less than 50 μm, phase change starts with an immediate eruption of vapor, generating mist flow instantaneously. In this study, Zhang et al. studied phase change in flat walls and subsequently tested the effect of varying the surface tension of the water. They studied a channel with a hydraulic diameter of 113 μm, as well as one with a hydraulic diameter of 44 μm. When initial nucleation begins at a temperature below boiling temperature, a small plateau is observed in the boiling curve. Bubble departure causes the formation of annular flow, which increases the heat transfer coefficient. When boiling occurs, two-phase annular flow is dominant in the channel, producing a very high heat transfer coefficient, thus a second plateau appears in the boiling curve. For the channel with a hydraulic diameter of 44 μm, the boiling curves show no boiling plateau, which is indicative of the sudden eruption of vapor and the development of mist flow, as mentioned earlier. However, mist flow has a smaller heat transfer coefficient compared to that of annular flow, and wall temperatures continue to increase as the heat fluxes are increased. Varying the surface tension did not show any significant effect on the two-phase flow behavior for flat walls. Four channels with enhanced walls, that is, walls with cavities, were also studied. The channels had hydraulic diameters between 28 and 73 μm, and the working fluid used was DI water. Unlike the flat-walled channels with hydraulic diameters less than 100 μm, the enhanced

wall channels did show the development of annular flow, since the cavities at the bottom of the channels caused the appearance of bubbles by trapping the gas.

Hestroni et al. [31] investigated the performance of a two-phase microchannel heat sink by attempting to maintain the operating temperature low at temperatures ranging from 323 to 333 K. The coolant used was the dielectric liquid DuPont Vertrel XF (dihydrodecafluoropentane $C_5H_2F_{10}$). The heat sink was composed of isosceles triangle microchannels with hydraulic diameters of 130 μm and a base angle of 55°. The thermal pattern of the heated surface of the sink showed a more uniform temperature distribution when compared to liquid water microchannel heat sinks. They observed that increasing the coolant flow rate increases the input wall heat flux, as well as the heat transfer coefficient. However, at the same mass velocity, the heat transfer coefficient is reduced when the heat flux and the vapor quality increase provided that x is small. The largest difference in surface temperature with Vertrel XF was 4–5 K, compared to 20 K for single-phase water. For water, 2.5 times the mass flow rate of Vertrel XF is required to achieve the same temperature difference of 5 K. Flow instabilities were observed and were attributed to variations in the pressure drop and a reduction in the heat transfer coefficient. Temperature fluctuations were also detected and were credited to the pressure drop fluctuations. Hestroni et al. attributed the fluctuations to the formation of vapor. As the heat flux increases, the vapor quality also rises, and so the amplitudes of the pressure and temperature fluctuations increase as well. For single-phase flow, the pressure drop increases slightly with increasing temperature. However, when the maximum device temperature exceeds the saturation temperature of the coolant, two-phase flow occurs, and the pressure drop rises accordingly.

Koo et al. [32] conducted a theoretical study of two-phase microchannel heat sinks, investigating the effect of microchannel hydraulic diameter and nonuniform heat fluxes on a two-phase microchannel heat sink's cooling capacity. Their theoretical model considered rectangular microchannels with hydraulic diameters ranging from 150 to 450 μm. The volume flow rate of the water ranged between 10 and 20 ml/min, yielding a mass quality between 0.25 and 0.5 at the exit of the channel. The exit pressure was fixed at 0.3 bar, so that the saturation temperature is approximately 70°C, while the inlet liquid temperature is fixed at 69°C. The saturation temperature decreases with increasing hydraulic diameter, while convective thermal resistance increases with increasing hydraulic diameter. Wider channels yield lower wall temperatures, but can also produce lateral instability heat transfer, which is undesirable. To investigate the effect of nonuniform wall heat flux, Koo et al. simulated two cases. Case 1 assumed 25% of the total heat flux is applied upstream, while Case 2 assumes that 75% of the total heat flux is located upstream. The wall temperature profiles for both cases show that the maximum temperature is located near the entrance of the channels as shown in Figure 7. Case 1 seems to be preferable because it produces a smaller pressure drop, lower average wall temperature, and a more uniform wall temperature distribution. Koo et al. speculated that the best two-phase heat sinks have 80% of the total heat flux applied downstream, because as more heat is applied to the latter half of the channel, the two-phase region becomes shorter, and so the pressure drop decreases. A hotspot measuring 2 mm long with 40% of the total heat concentrated within it was also considered. When the hotspot is near the inlet, boiling occurs near the inlet, thus the two-phase region becomes longer and the pressure drop increases. As the hotspot moves further down the channel, the maximum temperature decreases at a faster rate than the average sink temperature.
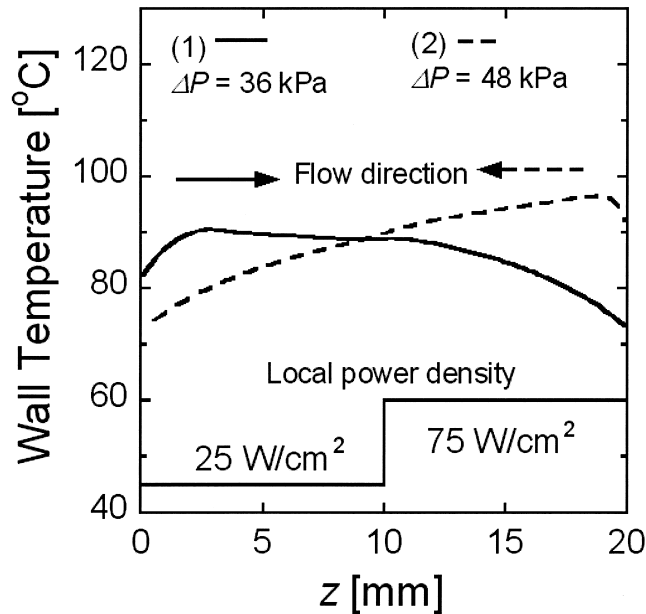
Figure 7. Wall temperature distribution for nonuniform wall heat fluxes [32].

In a very recent study, Qu and Mudawar [33] conducted an experimental study on a microchannel heat sink composed of 21 channels, and compared their results to correlations presented in Table 2. Each individual microchannel had a 231×713 μm cross-sectional area. Deoionized water was used as the working fluid at mass velocities ranging from 135 to 402 kg/m^{2}s. Inlet temperatures of 30°C and 60°C were used and the outlet pressure was fixed at 1.17 bar. They compared their results correlations 1 to 6 presented in Table 2, which were developed from boiling experimental data in conventional sized channels. Their results are presented in Figure 8, from which they observed that the experimental results were not at all in agreement with the correlations. Correlations at the macroscale indicate that the two-phase heat transfer coefficient, h_{tp}, increases with increasing thermodynamic equilibrium quality, x_e, while the experimental data indicates otherwise. Also, the macroscale correlations underpredict h_{tp} for low values of x_e and overpredict h_{tp} for high x_e. In Figure 9, the experimental data is compared to correlations 7 to 11 presented in Table 2, which were derived from boiling heat transfer data in mini/micro channels. It can be seen that only correlation 11 correctly follows the trend of the experimental data with a mean absolute error of 25.4%. In Part II of the study, Qu and Mudawar developed an annular two-phase model in order to predict the saturated boiling heat transfer coefficient at the microscale level. The model was based on the annular flow since it is the dominant two-phase flow pattern in microchannels. Their new model correctly predicted the trend of the experimental data presented in both Figures 8 and 9. The mean absolute error for the model was 13.3%, rendering it an effective tool for predicting two-phase flow behavior in microchannels. Qu and Mudawar emphasize that this model is not suitable for flow in macrochannels, since it is based on characteristics unique to microchannel flow only.

Table 2. Correlations used for comparison by Qu and Mudawar

Correlation	Reference from Qu and Mudawar [33]	Heat transfer coefficient, h_{tp}	MAE (%)
1	Chen [8], Edelstein et al. [30]	$h_{tp} = \dfrac{Nu_3}{Nu_4}(Eh_{sp} + Sh_{nb})$ $h_{sp} = 0.023(Re_f)^{0.8}(Pr_f)^{0.4}\dfrac{k_f}{d_h}$, $h_{nb} = 0.00122\left(\dfrac{k_f^{0.79}c_{P,f}^{0.45}v_g^{0.24}}{\sigma^{0.5}\mu_f^{0.29}h_{fg}^{0.24}v_f^{0.49}}\right)\Delta T_{sat}^{0.24}\Delta p_{sat}^{0.75}$ $E = \left(1 + \dfrac{1}{x_{tt}^{0.5}}\right)^{1.78}$, $S = 0.9622 - 0.5822\left[\tan^{-1}\left(\dfrac{Re_f E^{1.25}}{6.18\times10^4}\right)\right]$ $Re_f = \dfrac{G(1-x_e)d_b}{\mu_f}$, $Pr_f = \dfrac{c_{P,f}\mu_f}{k_f}$, $X_{tt} = \left(\dfrac{1-x_e}{x_e}\right)^{0.9}\left(\dfrac{v_f}{v_g}\right)^{0.5}\left(\dfrac{\mu_f}{\mu_g}\right)^{0.1}$	43.9
2	Shah [9, 31]	$h_{tp} = \dfrac{Nu_3}{Nu_4}\max(E, S)h_{sp}$ $h_{sp} = 0.023(Re_f)^{0.8}(Pr_f)^{0.4}\dfrac{k_f}{d_h}$ For $NN > 1.0$, $S = 1.8/NN^{0.8}$, $E = 230Bo^{0.5}$ (Bo $> 3\times10^{-5}$) or $E = 1 + 46Bo^{0.5}$ (Bo $< 3\times10^{-1}$) For $0.1 < NN \leqslant 1.0$, $S = 1.8/NN^{0.8}$, $E = FBo^{0.5}\exp(2.47NN^{-0.15})$ For $NN \leqslant 0.1$, $S = 1.8/NN^{0.8}$, $E = FBo^{0.5}\exp(2.47NN^{-0.15})$ $F = 14.7(Bo \geqslant 11\times10^{-4})$ or $F = 15.43(Bo < 11\times10^{-4})$ $NN = Co(Fr_f \geqslant 0.04)$ or $NN = 0.38Fr_f^{-0.3}Co(Fr_f < 0.04)$ $Co = \left(\dfrac{1-x_e}{x_e}\right)^{0.8}\left(\dfrac{v_f}{v_g}\right)^{0.5}$, $Fr_f = \dfrac{v_f^2 G^2}{gd_h}$	53.7
3	Gungor and Winterton [32]	$h_{tp} = \dfrac{Nu_3}{Nu_4}(Eh_{sp} + Sh_{nb})$ $h_{sp} = 0.023(Re_f)^{0.8}(Pr_f)^{0.4}\dfrac{k_f}{d_h}$, $E = 1 + 24000Bo^{1.16} + 1.37\left(\dfrac{1}{X_u}\right)^{0.86}$	50.1

4	Kandlikar [15]	$h_{nb} = 55P_r^{0.12}(-\log_{10}(P_r))^{-0.55}M_W^{-0.5}q_{ch}''^{0.67}$, $S = (1 + 1.15\times10^{-6}E^2 Re_f^{1.17})^{-1}$ If $Fr_f \leq 0.05$, replace E by $EFr_f^{0.1-2Fr_f}$ and S by $SFr_f^{0.5}$, respectively $h_{tp} = \dfrac{Nu_3}{Nu_4}\max(E,S)h_{sp}$ $h_{sp} = 0.023(Re_f)^{0.8}(Pr_f)^{0.4}\dfrac{k_f}{d_h}$, $E = 0.6683Co^{-0.2}f(Fr_f) + 1058Bo^{0.7}$ $S = 1.136Co^{-0.9}f(Fr_f) + 667.2Bo^{0.7}$ $f(Fr_f) = 1(Fr_f \geqslant 0.04)$ or $f(Fr_f) = (25Fr_f)^{0.3}(Fr_f < 0.04)$	49.4
5	Liu and Winterton [33]	$h_{tp} = \dfrac{Nu_3}{Nu_4}((Eh_{sp})^2 + (Sh_{nb})^2)^{0.5}$ $h_{sp} = 0.023(Re_{fo})^{0.8}(Pr_f)^{0.4}\dfrac{k_f}{d_h}$, $E = \left[1 + x_e Pr_f\left(\dfrac{v_g}{v_f} - 1\right)\right]^{0.35}$, $Re_{fo} = \dfrac{Gd_h}{\mu_f}$ $h_{nb} = 55P_r^{0.12}(-\log_{10}(P_r))^{-0.55}M_W^{-0.5}q_{ch}''^{0.67}$, $S = (1 + 0.055E^{0.1}Re_{fo}^{0.16})^{-1}$ If $Fr_f \leq 0.05$, replace E by $EFr_f^{0.1-2Fr_f}$ and S by $SFr_f^{0.5}$, respectively	35.1
6	Steiner and Taborek [34]	$h_{tp} = \dfrac{Nu_3}{Nu_4}[(Eh_{sp})^3 + (Sh_{nb})^3]^{1/3}$ $h_{sp} = 0.023(Re_{fo})^{0.8}(Pr_f)^{0.4}\dfrac{k_f}{d_h}$, $E = [(1 - x_e)^{1.5} + 1.9x_e^{0.6}(v_g/v_f)^{0.35}]^{1.1}$ $h_{nb} = 25.581$ W/m²K, $S = F\left(\dfrac{q_{ch}''}{1.5\times10^5}\right)^{0.8-0.1\exp(1.75Pr)}\left(\dfrac{d_h}{0.01}\right)^{-0.4}f(M_W)$ $F = 2.816P_r^{0.45} + \left[3.4 + \dfrac{1.7}{1 - P_r^7}\right]P_t^{3.7}$, $f(M_W) = 0.72$	46.2
7	Lazarek and Black [7]	$h_{tp} = \dfrac{Nu_3}{Nu_4}\left[30(Re_{fo})^{0.857}(Bo)^{0.714}\dfrac{k_f}{d_h}\right]$	36.2

(continued)

Table 2. (*Continued*)

| Correlation	Reference from Qu and Mudawar [33]	Heat transfer coefficient, h_{tp}	MAE (%)
8	Tran et al. [11]	$h_{tp} = \dfrac{\mathrm{Nu}_3}{\mathrm{Nu}_4}\left[8.4\times10^5\,(\mathrm{Bo}^2 We_f)^{0.3}\left(\dfrac{v_g}{v_f}\right)^{-0.4}\right],\quad We_f = \dfrac{v_f G^2 d_h}{v}$	98.8
9	Lee and Lee [18]	$h_{tp} = \dfrac{\mathrm{Nu}_3}{\mathrm{Nu}_4}(E h_{sp})$ $h_{sp} = \mathrm{Nu}_4\dfrac{k_f}{d_h},\quad E = 10.3\beta^{0.398}\phi_f^{0.598}$ $\phi_f = \left(1 + \dfrac{C}{x_{vt}} + \dfrac{1}{X_{vt}^2}\right)^{0.5},\quad C = 6.185\times10^{-2}\mathrm{Re}_{fo}^{0.726}$ $X_{vt} = \left(\dfrac{f_f}{f_g}\right)^{0.5}\left(\dfrac{1-x_e}{x_e}\right)\left(\dfrac{v_f}{v_g}\right)^{0.5},\quad f_g = \dfrac{0.079}{\mathrm{Re}_g^{0.25}},\quad \mathrm{Re}_g = \dfrac{Gx_o d_h}{\mu_g}$ $f_f = \dfrac{24}{\mathrm{Re}_f}(1 - 1.355\beta + 1.947\beta^2 - 1.701\beta^3 + 0.956\beta^4 - 0.254\beta^5)$ $\beta = \dfrac{W_{ch}}{H_{ch}}$	272.1
10	Yu et al. [19]	$h_{tp} = \dfrac{\mathrm{Nu}_3}{\mathrm{Nu}_4}\left[6.4\times10^6\,(\mathrm{Bo}^2 We_f)^{0.24}\left(\dfrac{v_g}{v_f}\right)^{-0.2}\right]$	19.3
11	Warrier et al. [20]	$h_{tp} = \dfrac{\mathrm{Nu}_3}{\mathrm{Nu}_4}(E h_{sp})$ $h_{sp} = \mathrm{Nu}_4\dfrac{k_f}{d_h},\quad E = 1.0 + 6\mathrm{Bo}^{1/16} + f(\mathrm{Bo})x_e^{0.65}$ $f(\mathrm{Bo}) = -5.3(1 - 855\mathrm{Bo})$	25.4

From Qu and Mudawar [33].
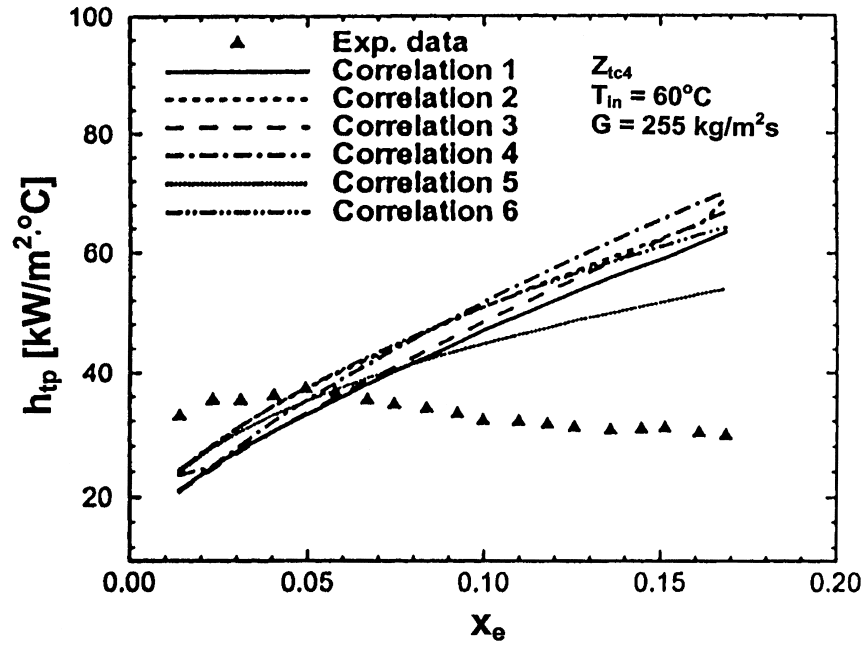
Figure 8. Comparison of experimental data for the two-phase heat transfer coefficient in microchannels with correlations for macrochannels [33].
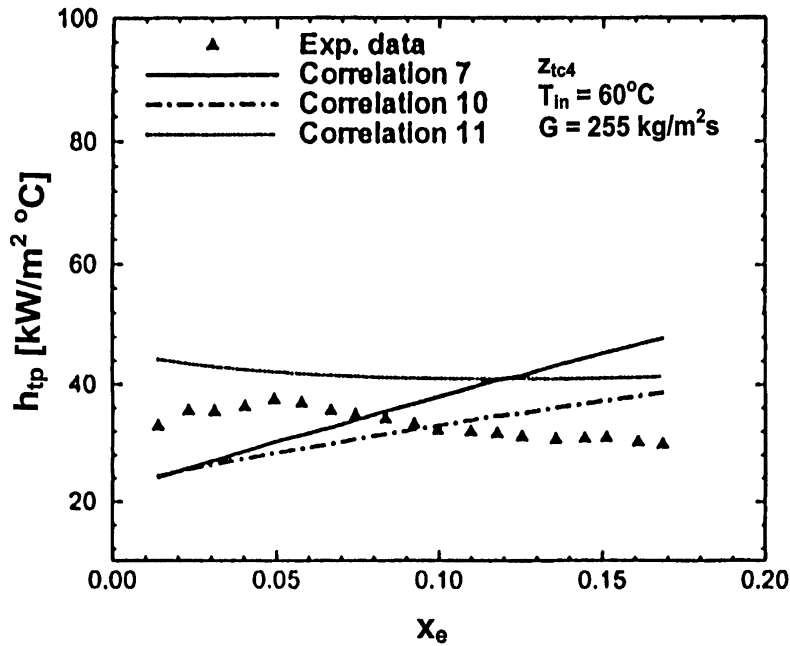

Figure 9. Comparison of experimental data for the two-phase heat transfer coefficient with correlations for mini/microchannels [33].

SUMMARY AND FUTURE DIRECTIONS

This paper has provided an overview of the research performed thus far in the field of microchannel heat sinks. There are many other research fields concerning microchannel heat sinks that have yet to be explored. This section will summarize the possible future directions of research that may be followed in order to obtain greater understanding of these microdevices.

Effect of coolant types should be investigated more thoroughly. Liquids seem to provide superior cooling properties when compared to gases, since they offer lower thermal resistance. Water has been the coolant of choice for most experiments because it is readily available and cheap and has a high specific heat capacity. Yet, still the effect of the type of the liquid used is not studied. CFD packages could be used to simulate various types of coolants and help predict which one provides better cooling capabilities at affordable costs. Experiments may be performed later to validate the simulations' results.

Surface roughness within the microchannel seems to have a significant effect on flow behavior at the microscale. Flow transition from laminar flow to turbulent flow at the microscopic level must be studied in greater details so that one may accurately predict at which value of Reynolds number this transition occurs for all wall roughnesses. Zeighami et al.'s [5] results showed that for microchannels the transition Reynolds number is apparently lower than that at the macro-level. Guo and Li [8] showed that this lower transition Reynolds number is due to the wall roughness inside the microchannel. Experiments using different wall roughnesses should be conducted in the future in order to obtain better understanding of the effect of friction on the performance of microchannel heat sinks.

The optimization of microchannel heat sink dimensions is still in its primary research. This optimization should ensure low and uniform temperature distribution, as well as low pressure drops. Perret et al. [18] developed an optimization model that yielded optimized parameters for the best performance single-phase liquid microchannel heat sink. However, this is but one optimization model. In the case of two-phase microchannel heat sinks, Koo et al. [32] developed their own model, observing that narrower microchannels provide higher local heat transfer coefficients for both the liquid and vapor phases of the fluid and that wider channels seem to show lateral heat transfer instabilities although they yield lower wall temperatures. These two models pave the way for upcoming optimization models that will guarantee the maximum performance of future microchannel heat sinks.

Boiling instabilities in two-phase microchannel heat sinks should be studied thoroughly. Instabilities were observed and were attributed to large pressure drops. Lateral instabilities also exist in wide microchannels. The fluid was observed to revert back to liquid upon boiling, and to begin boiling once again in cycles that last up to a few minutes. Hestroni et al. [31] noticed erratic pressure and temperature variations in two-phase microchannel heat sinks. These instabilities will hinder the implementation of microchannel heat sinks in commercial applications as long as they exist unexplained.

Microchannel heat sinks that involved phase change from liquid to vapor experienced different behaviors. Some of the boiling curves generated in two-phase microflows exhibited no boiling plateaus, while others did. First, this was attributed to the microchannel dimensions as it was thought that the micro size of the channels prevents bubble formation. Yet this was proven untrue as boiling did occur in microchannels with enhanced surfaces containing cavities, which provided nucleation spots for the bubbles to

form. The existence of the boiling plateau is of great importance as it allows the removal of high amounts of heat at relatively low and constant temperatures. Further testing on two-phase flow in microchannels of hydraulic diameters less than 100 μm should be performed to determine whether the boiling plateaus in the boiling curves generally do not exist for microchannels of these sizes.

Different microchannel geometries should be tested to see if one shape in particular yields a better cooling performance. Experimental data for different geometries should be tested for two-phase flow in order to generate accurate flow regime maps that may be able to predict the flow pattern. Transitional flow regimes should also be clearly and universally defined in experiments in order to avoid confusion when attempting to model the flow regime maps. This experimental data will also be useful in generating models that may predict the heat transfer coefficient associated with two-phase flow in microchannels.

Fluid properties are affected by variations in temperature; however, most of the studies cited did not consider this fact. Studies accounting for the temperature-dependent fluid properties will certainly give more accurate and realistic results than constant fluid properties studies, thus predicting the real performance of microchannel heat sinks.

Spatially varying heat fluxes should be investigated further in the future. There was but one study that assumed spatially varying heat fluxes, which concluded that the best two-phase microchannel heat sinks have 80% of the total heat flux applied to the latter half of the channel. Future work might provide other nonuniformity patterns that may enhance microchannel heat sink performance.

REFERENCES

1. D. B. Tuckerman and F. R. Pease, Microcapillary Thermal Interface Technology for VLSI Packaging, *Digest of Technical Papers—Symposium on VLSI Technology*, Maui, HI, pp. 60–61, 1983.
2. D. B. Tuckerman, *Heat-Transfer Microstructures for Integrated Circuits*, Ph.D. thesis, Stanford University, 1984.
3. S. T. Poh and E. Y. K. Ng, Heat Transfer and Flow Issues in Manifold Microchannel Heat Sinks: A CFD Approach, *Proc. Electronic Packaging Technology Conference, EPTC*, pp. 246–250, 1998.
4. K. Kawano, K. Minakami, H. Iwasaki, and M. Ishizuka, Microchannel Heat Exchanger for Cooling Electrical Equipment, *Proc. ASME Heat Transfer Division*, vol. 3, pp. 173–180, 1998.
5. R. Zeighami, D. Laser, P. Zhou, M. Asheghi, S. Devasenathipathy, T. Kenny, J. Santiago, and K. Goodson, Experimental Investigation of Flow Transition in Microchannels Using Micron-Resolution Particle Image Velocimetry, *Proc. 7th Intersociety Conference on Thermomechanical Phenomena in Electronic Systems*, ITHERM, vol. 2, pp. 148–153, 2000.
6. M. M. Rahman, Measurements of Heat Transfer in Microchannel Heat Sinks, *International Communications in Heat and Mass Transfer*, vol. 27, no. 4, pp. 495–506, 2000.
7. Z.-X. Li, D. X. Du, and Z.-Y. Guo, Experimental Study on Flow Characteristics of Liquid in Circular Microtubes, *Proc. International Conference on Heat Transfer and Transport Phenomena in Microscale*, pp. 162–167, 2000.
8. Z.-Y. Guo and Z.-X. Li, Size Effect on Single-Phase Channel Flow and Heat Transfer at Microscale, *International Journal of Heat and Fluid Flow*, vol. 24, pp. 284–297, 2003.
9. P. Gao, S. Le Person, and M. Favre-Marinet, Scale Effects on Hydrodynamics and Heat Transfer in Two-Dimensional Mini and Microchannels, *International Journal of Thermal Sciences*, vol. 41, pp. 1017–1027, 2002.

10. R. R. Riehl, P. Seleghim, Jr., and J. M. Ochterbeck, Comparison of Heat Transfer Correlations for Single- and Two-Phase Microchannel Flows for Microelectronics Cooling, *Proc. Intersociety Conference on Thermomechanical Phenomena in Electronic Systems*, ITHERM, pp. 409–416, 1998.

11. X. F. Peng and B. X. Wang, Forced Convection and Flow Boiling Heat Transfer for Liquid Flowing through Microchannels, *International Journal of Heat and Mass Transfer*, vol. 36, no. 14, pp. 3421–3427, 1993.

12. B. X. Wang and X. F. Peng, Experimental Investigation on Liquid Forced-Convection Heat Transfer through Microchannels, *International Journal of Heat and Mass Transfer*, vol. 37, no. 1, pp. 73–82, 1994.

13. X. F. Peng and G. P. Peterson, The Effect of Thermofluid and Geometrical Parameters on Convection of Liquids through Rectangular Microchannels, *International Journal of Heat and Mass Transfer*, vol. 38, no. 4, pp. 755–758, 1995.

14. X. F. Peng and G. P. Peterson, Convective Heat Transfer and Flow Friction for Water Flow in Microchannel Structures, *International Journal of Heat and Mass Transfer*, vol. 39, no. 12, pp. 2599–2608, 1996.

15. E. Y. K. Ng, C. P. Tso, Z. M. Wen, and K. F. Choo, Numerical Simulation of Flow and Conjugate Heat Transfer in a Microchannel for Electronics Cooling, *Journal of Electronics Manufacturing*, vol. 9, no. 2, pp. 141–153, 1999.

16. A. G. Fedorov and R. Viskanta, Analysis of Conjugate Heat Transfer in a Three-Dimensional Microchannel Heat Sink for Cooling of Electronic Components, *Proc. ASME Heat Transfer Division*, vol. 364–363, pp. 89–98, 1999.

17. A. G. Fedorov and R. Viskanta, Three-Dimensional Conjugate Heat Transfer in the Microchannel Heat Sink for Electronic Packaging, *International Journal of Heat and Mass Transfer*, vol. 43, no. 3, pp. 399–415, 2000.

18. C. Perret, J. Boussey, C. Schaeffer, and M. Coyaud, Analytic Modeling, Optimization, and Realization of Cooling Devices in Silicon Technology, *IEEE Transactions on Components and Packaging Technologies*, vol. 23, no. 4, pp. 665–672, 2000.

19. Z.-Y. Guo and X. B. Wu, Compressibility Effect on the Gas flow and Heat Transfer in a Microtube, *International Journal of Heat and Mass Transfer*, vol. 40, pp. 3251–3254, 1997.

20. Z.-Y. Guo and X. B. Wu, Further Study on the Compressibility Effect on the Gas Flow and Heat Transfer in a Microtube, *Microscale Thermophysical Engineering*, vol. 2, pp. 111–120, 1998.

21. M. J. Marongiu, Compressibility Effects in the Design of Gas-Cooled Microchannel Heat Sinks, *Proc. 5th Intersociety Conference on Thermal Phenomena in Electronic Systems*, pp. 124–129, 1996.

22. M. J. Marongiu, B. Kusha, and G. S. Fallon, Compressible Gas-Cooled Micro-Channel Heat Sink Board (Substrates), *Proc. 1998 International Symposium on Microelectronics*, vol. 3582, pp. 856–861, 1998.

23. A. Beskok and G. Karniadakis, A Model for Flows in Channels, Pipes, and Ducts at Micro and Nano Scales, *Microscale Thermophysical Engineering*, vol. 3, no. 1, pp. 43–77, 1999.

24. G. Karniadakis and A. Beskok, *Micro Flows: Fundamentals and Simulation*, Springer-Verlag, New York, 2002.

25. J. Baker and M. E. Calvert, Effect of Variable Viscosity on Coupled Heat and Momentum Transfer in Microchannel Flows, *American Society of Mechanical Engineers, Fluids Engineering Division (Publication) FED*, vol. 237, no. 2, pp. 775–782, 1996.

26. L. Jiang, M. Wong, and Y. Zohar, Phase Change in Microchannel Heat Sinks with Integrated Temperature Sensors, *Journal of Microelectromechanical Systems*, vol. 8, no. 4, pp. 358–365, 1999.

27. L. Jiang, M. Wong, and Y. Zohar, Forced Convection Boiling in a Microchannel Heat Sink, *Journal of Microelectromechanical Systems*, vol. 10, no. 1, pp. 80–87, 2001.

28. J. Koo , L. Jiang, L. Zhang, P. Zhou, S. Banerjee, T. Kenny, J. Santiago, and K. Goodson, Modeling of Two-Phase Microchannel Heat Sinks for VLSI Chips, *Proc. 14th IEEE International Conference on Micro Electro Mechanical Systems (MEMS) 2001*, pp. 422–426, 2001.

29. L. Zhang, J. Koo, L. Jiang, M. Asheghi, K. Goodson, J. G. Santiago, and T. Kenny, Measurements and Modeling of Two-Phase Flow in Microchannels with Nearly Constant Heat Flux Boundary Conditions, *Journal of Microelectromechanical Systems*, vol. 11, no. 1, pp. 12–19, 2002.

30. L. Zhang, E. Wang, J. Koo, L. Jiang, K. Goodson, J. Santiago, and T. Kenny, Enhanced Nucleate Boiling in Microchannels, *Proc. 15th IEEE International Conference on Micro Electro Mechanical Systems (MEMS) 2002*, pp. 89–92, 2002.

31. G. Hestroni, A. Mosyak, Z. Segal, and G. Ziskind, A Uniform Temperature Heat Sink for Cooling of Electronic Devices, *International Journal of Heat and Mass Transfer*, vol. 45, no. 16, pp. 3275–3286, 2002.

32. J. Koo, L. Jiang, A. Bari, L. Zhang, and E. Wang, Convective Boiling in Microchannel Heat Sinks with Spatially Varying Heat Generation, *Thermomechanical Phenomena in Electronic Systems–Proceedings of the Intersociety Conference*, pp. 341–346, 2002.

33. W. Qu and I. Mudawar, Flow Boiling Heat Transfer in Two-Phase Micro-Channel Heat Sinks: Part I: Experimental Investigation and Assessment of Correlation Methods. Part II: Annular Two-Phase Flow Model, *International Journal of Heat and Mass Transfer*, vol. 46, pp. 2755–2784, 2003.